Astrochronology and radio-isotopic dating of the Alano di Piave section (NE Italy), candidate GSSP for the Priabonian Stage (Late Eocene)

Simone Galeotti[a], Diana Sahy[b], Claudia Agnini[c], Daniel Condon[b], Eliana Fornaciari[c], Federica Francescone[a], Luca Giusberti[c], Heiko Pälike [d], David J.A. Spofforth [e], Domenico Rio[c]

[a] Dipartimento di Scienze Pure e Applicate, Università degli Studi di Urbino Carlo Bo, Campus Scientifico "E. Mattei," 61029 Urbino, Italy

[b] British Geological Survey, Keyworth, NG12 5GG, United Kingdom

[c] Dipartimento di Geoscienze, Università di Padova, via G. Gradenigo, 6, 35131 Padova (Italy)

[d] MARUM–Center for Marine Environmental Sciences, University of Bremen, Leobener Strasse, 28359 Bremen, Germany

[e] CGG MCNV (GeoSpec), Llandundo, LL30 1SA, UK

Abstract: We have carried out an integrated chronostratigraphic analysis of the Alano di Piave section, proposed GSSP for the Bartonian/Priabonian boundary (Late Eocene). Age constraints were derived independently from a floating cyclochronology based on carbon isotope and wt.% $CaCO_3$ records, and $^{206}Pb/^{238}U$ dating of zircons from four volcanic tuffs. Orbital and radio-isotopic estimates of the duration of intervals bracketed by consecutive crystal-rich volcanic tuff layers are in good overall agreement, but discrepancies of 40 – 160 kyr are present between nominal volcanic tuff dates derived from astrochronology and $^{206}Pb/^{238}U$. The degree to which these discrepancies are statistically significant at the 2σ level depends on the interpretation of the U-Pb zircon data, and the uncertainties assigned to the astronomical age model. The possible source and significance of these discrepancies are explored in detail. The resulting age model, combined with published bio-, and magnetostratigraphic data, is used to establish the duration of individual magnetochrons in the interval spanning the Bartonian/Priabonian transition, and the timing of late Bartonian-early Priabonian biostratigraphic and magnetostratigraphic events relative to the proposed GSSP, the regionally traceable crystal-rich tuff layer "Tiziano Bed". The chronostratigraphic framework developed at Alano di Piave will facilitate the global correlation of the Priabonian GSSP based on both bio- and magnetostratigraphic criteria. The obtained astrochronology allows a precise correlation of the Alano di Piave $\delta^{13}C$ record with oceanic successions confirming a strong dependency of the marine carbon cycle on astronomical forcing although with inter-site differences, which could be related to water mass organization.

Keywords: Integrated Stratigraphy; Carbon isotopes; Priabonian; GSSP; Alano di Piave

1. Introduction

The Alano di Piave section has been presented at the International Subcommission on Paleogene Stratigraphy (ISPS) as a potential candidate for defining the global boundary stratotype section and point (GSSP) of the late Eocene Priabonian Stage. The interdisciplinary stratigraphic analysis carried out by an *ad hoc* working group provided a robust integrated stratigraphic framework for the section, which proved to be suitable for calcareous plankton biostratigraphy and magnetostratigraphy. Here we complement the already existing data by adding a cyclostratigraphic dating of the interval spanning the Bartonian/Priabonian boundary, coupled with $^{206}Pb/^{238}U$ dating of zircon from crystal-rich volcanic tuffs intercalated in the Alano di Piave record. Independently of the decision on which criterion to select for the definition of the GSSP, which will eventually be voted by the Paleogene Subcommission of the International Commission on Stratigraphy, we aim at providing a tool for a high resolution, i.e. precession scale, calibration of events with respect to the base of the Priabonian stage by developing a floating cyclochronology. Further, we tune the obtained cyclostratigraphy to the available astronomical solution, providing an astrochronological age for bio- and magnetostratigraphic event, as well as regional lithostratigraphic markers.

2. Geological and Stratigraphic setting

The section is located in the Southern Alps of the Veneto region (NE Italy), which is the type area of the Priabonian, being exposed along the banks of the Calcino torrent, near the village of Alano di Piave (Fig. 1). It consists of ~120–130 m of bathyal gray marls interrupted in the lower part by an 8-m-thick package of laminated dark to black marlstones. Intercalated in the section, there are eight prominent marker beds, six of which are crystal-rich tuff layers, whereas the other two are bioclastic rudites. These distinctive layers are useful for regional correlation and for an easy recognition of the various intervals of the section. Tuff layers are coeval with similar beds cropping out in the Giudicarie Belt area, which have been interpreted to correlate with volcanic rocks of the Paleogene Veneto volcanic province or an "Adamello-related" volcanic activity (e.g., Sciunnach and Borsato, 1994; Beccaluva et al., 2007). The section is easily accessible, crops out continuously, is unaffected by any structural deformation, is rich in calcareous plankton, and contains an expanded record of the critical interval for defining the GSSP of the Priabonian. The stratigraphic completeness of the record is supported by integrated high-resolution calcareous plankton biostratigraphy and detailed magnetostratigraphy (Agnini et al., 2011, 2014) (Fig. 2). Here, we integrate these data with a new cyclostratigraphic model and radio-isotopic data that provide a strong chronological framework and would eventually give all the elements to discuss the criteria that should be used for driving the choice of the GSSP of the Priabonian Stage (e.g., Agnini et al., 2011, 2014).

3. Material and Methods

Spectral analysis based on wavelet and the Multi Taper Method (MTM) has been carried out on the $\delta^{13}C$ record of Spofforth et al. (2010) and the wt.% $CaCO_3$ data from their isotope runs (Fig. 2). The latter record was supplemented by additional wt.% $CaCO_3$ data obtained using a "Dieter-Fruhling" calcimeter (with a precision of 1.5% based on replicate analyses) for the interval between 40-85 m, which brackets the Bartonian-Priabonian transition. Spectral analysis of the $\delta^{13}C$ record has been conducted on the interval spanning 40–104 m, corresponding to the uppermost C18n.1n to the lowermost C16r (Agnini et al., 2011). Spectral analysis of the wt.% $CaCO_3$ record has been performed on the interval spanning 40–85 m, spanning the uppermost C18n.1n to the middle C17n.1n (Agnini et al., 2011) (Fig. 2). MTM has been performed after 2nd order polynomial detrending of the $\delta^{13}C$ record using the Astrochron Package (Meyers, 2014). Moreover, Evolutive Harmonic Analysis (EHA) has been performed on the $\delta^{13}C$ record to recognise the frequency modulation of the eccentricity components (e.g. Laurin et al., 2016; Galeotti et al., 2017).

U-Pb dating of zircons from four volcanic tuffs intercalated in the Alano di Piave record (Fig. 2) was carried out at the NERC Isotope Geosciences Laboratory (NIGL), British Geological Survey, via chemical abrasion – isotope dilution – thermal ionization mass spectrometry (CA-ID-TIMS). Zircons were separated from each sample using conventional mineral separation techniques. The selection of zircon grains and grain fragments for ID-TIMS analyses was based on a combination of crystal morphology, with preference given to clear, euhedral grains, and cathodoluminescence (CL) imaging of the equatorial section of epoxy-mounted zircons to isolate crystals or crystal fragments likely to be representative of the eruption age of each sample. Analytical protocols followed the methodology of Sahy et al. (2015), with the main points briefly outlined here. All samples were subject to a modified version of the chemical abrasion protocol of Mattinson (2005) to remove crystal volumes affected by open system behaviour through Pb-loss. All samples were spiked with the gravimetrically calibrated EARTHTIME ET535 or ET2535 isotopic tracers (Condon et al., 2015; McLean et al., 2015). Raw U and Pb data were filtered using the Tripoli application (Bowring et al., 2011). Dates and propagated random and systematic uncertainties were calculated in ET-Redux (McLean et al., 2011) using the U decay constants of Jaffey et al. (1971) and the $^{238}U/^{235}U$ ratio of Hiess et al. (2012). All U-Pb radio-isotopic data have been archived using the EARTHCHEM/EARTHTIME Geochron data base (Bowring et al., 2011).

4. Results and discussion

4.1 U-Pb dating results

A total of 40 zircon crystals and crystal fragments were analysed, 23 of which were selected based on CL imaging (Fig. 3) with tabulated results included in the Supplementary Information (Table S1). Analytical uncertainties on $^{206}Pb/^{238}U$ dates ranged between 0.023-0.088 Myr (0.06-0.24%), with a mean of 0.046 Myr (0.12%) (all U-Pb age uncertainties are quoted at the 2σ level). Each grain contained between 5 and 134 pg of radiogenic Pb (on average 21 pg), with measured radiogenic to common Pb ratios (Pb^*/Pb_c) between 3 and 123. Zircon $^{206}Pb/^{238}U$ dates from each sample showed scatter over 0.20-0.55 Myr, in excess of analytical uncertainty. The dataset is free of non-reproducible young dates, which would be a typical manifestation of open-system behaviour through Pb-loss. Instead, data from each sample presents as a group of statistically equivalent 'young' dates (n= *4-7*), tailing into arrays of non-reproducible older dates (Fig. 3). This suggests that the chemical abrasion protocols applied prior to analysis have been successful in mitigating open system behaviour, although Pb-loss at a level that is masked by the 2σ analytical uncertainties of the youngest coherent group of measurements cannot be ruled out. We interpret these age distributions as resulting from a combination of prolonged zircon crystallization prior to eruption, the incorporation of older xenocrystic cores, and contamination with older detrital zircons during deposition or subsequent bioturbation (Bowring and Schmitz, 2003; Sageman et al., 2014; Schoene, 2014; Wotzlaw et al., 2014; Sahy et al., 2015, 2017). The interpretation of complex zircon

$^{206}Pb/^{238}U$ datasets in terms of eruption age is typically based on either the youngest measured date, or a weighted mean of the youngest statistically equivalent group of dates from each sample (Sageman et al., 2014, Sahy et al., 2015), possibly including additional constraints on the relative stratigraphic context of the samples to refine uncertainty estimates (Schoene, 2014, Wotzlaw et al., 2014). The choice of interpretive framework is somewhat subjective and must take into account the strengths and weaknesses of both approaches. The 'youngest grain' approach is based on the assumption that the youngest (reproducible) determined date most closely approximates the youngest grain and thus the eruption age of the tuff. However, an interpretation based on a single measurement from each sample disregards the essential role of reproducibility as a measure of the robustness of the interpretation, and fails to account for the analytical scatter expected around the true measured age. Conversely, the use of weighted means for coherent groups of young zircons is expected to average out analytical scatter, but similarly to the youngest grain approach, results may be biased towards younger or older values if geological scatter is present at a level that is masked by the respective 2σ analytical uncertainties. The use of weighted means further requires that a subjective decision be made regarding the number of analyses included in each mean age. This decision is typically guided by the mean square of the weighted deviates (MSWD), with the range of acceptable values dependent on the size of the population and the analytical uncertainties of each date (Wendt and Carl, 1991). Hereafter, dates calculated using this approach are referred to as acceptable-MSWD weighted means.

An alternative interpretive framework for zircon $^{206}Pb/^{238}U$ data has recently been proposed by Keller et al. (2018), who argued that, given the prolonged nature of zircon crystallisation in a magma chamber, and the shape of theoretical and empirical zircon crystallization distributions published in the literature (e.g. Watson et al., 1996; Keller et al., 2017; Samperton et al., 2017), radio-isotopic closure of even the youngest dated zircons from a volcanic tuff sample may not directly date the eruption age of that tuff at the resolution afforded by the analytical precision of state-of-the-art mass spectrometry. They further noted that the inclusion of numerous dates from a coherent group of ‘youngest’ zircons will artificially reduce the analytical uncertainty of the calculated weighted mean date. Instead, the approach of Keller et al. (2018) relies on Bayesian modelling based upon the range of measured $^{206}Pb/^{238}U$ dates from a tuff sample, coupled with a theoretical a-priori pre-eruptive zircon crystallization distribution, to approximate the eruption age. However, it should be noted that, in a manner similar to traditional acceptable-MSWD weighted mean age interpretations, this approach is open to bias through unrecognised Pb-loss (Keller et al. 2018), both of which may result in dates that post-date the ‘true’ eruption age. Unlike acceptable-MSWD weighted mean interpretations, the Bayesian approach is also susceptible to bias through the presence of outliers at the older end of the array of dates obtained from a tuff sample, which may pre-date the time when the source magma for a given tuff reached zircon saturation (e.g. post-depositional contamination with older zircons if background sedimentation includes reworked volcanoclastic material, Sahy et al. 2015).

Below we provide details of the interpretation of $^{206}Pb/^{238}U$ data from zircons from the four crystal-rich tuffs analysed in this study, both in terms of acceptable-MSWD weighted means, and using the Bayesian approach of Keller et al. (2018). Uncertainties are reported as ± X/Y/Z, where X is the analytical uncertainty, Y includes X and the uncertainty associated with the calibration of the EARTHTIME isotopic tracer, and Z includes Y and uncertainty associate with the ^{238}U decay constant. For weighted mean ages, Y and Z are calculated using the ET-Redux software package, while for Bayesian eruption ages they were calculated by adding 0.03% and 0.11% of the eruption age to the eruption age uncertainty in quadrature.

Single zircon U-Pb data and interpreted U-Pb ages both in terms of weighted means and following the Bayesian interpretation of Keller et al. (2018) are provided in Figure 3 and Table 1.

Ten zircon grains and grain fragments were analysed from the COL12-7248C sample (International Geo Sample Number, IGSN: IEDS1000O), five of which were pre-screened via CL-imaging, with $^{206}Pb/^{238}U$ dates ranging between 36.607 and 37.034 Ma. The youngest seven analyses gave a weighted mean age of 36.630 ± 0.013/0.017/0.043 Ma (MSWD=0.98). The data underpinning the weighted mean include replicate measurements from two CL-imaged grains (i.e. each grain was broken in half perpendicular to the long axis), which gave statistically equivalent results (fractions z6A and B, and z10A and B in Figure 3 and Table S1). The Bayesian approach of Keller et al. (2018) gave an eruption age of 36.593 ± 0.046/0.047/0.062 Ma. The oldest date from this sample is not reproducible, and appears to be an outlier. If we assume that all the analysed zircons from this sample are strictly autocrystic, this would imply that the data incompletely samples the zircon saturation distribution, which would result in an over-estimated eruption age (Keller et al., 2018). However, if the oldest date is assumed to reflect a xenocrystic zircon and is excluded from interpretation, the eruption age becomes 36.608 ± 0.028/0.030/0.050 Ma.

Eleven zircons were analysed from the Canaletto bed (IGSN: IEDS1000P), of which seven were CL-imaged. $^{206}Pb/^{238}U$ dates ranging between 36.763 and 36.962 Ma, with the youngest four grains yielding a weighted mean age of 36.794 ± 0.024/0.028/0.048 Ma (MSWD=1.2). The remaining seven older grains include replicate measurements of two CL-imaged zircons, z9A and B (two halves) and z7A and B (two tips, see Figure 3, and Supplementary Table S1), with each pair giving statistically equivalent results. This suggests that the scatter observed in the Alano di Piave dataset is due mostly to prolonged growth prior to eruption or bioturbation rather than the inheritance of older cores. Additionally, the two halves of fraction z9 gave equivalent dates which would not have been the case if a xenocrystic core was present, as the proportion of core to younger rim would likely have been different in the two halves of the grain. The Bayesian approach of Keller et al. (2018) gave an eruption age of 36.751 ± 0.064/0.065/0.076 Ma.

Nine zircon grains were analysed from the COL12-5229C sample (IGSN: IEDS1000Q), five of which were pre-screened via CL-imaging. $^{206}Pb/^{238}U$ dates ranged between 37.168 and 37.427 Ma. The weighted mean age of the youngest five grains is 37.197 ± 0.015/0.020/0.044 Ma (MSWD=0.96), and includes replicate measurements of a CL-imaged grain (two halves, A and B, of fraction z9, see Figure 3 and Supplementary Table S1) which gave statistically equivalent results.

The Bayesian approach of Keller et al. (2018) gave an eruption age of 37.154 ± 0.052/0.053/0.067 Ma.

Ten zircon grains and fragments, of which six were screened using CL imaging, were analysed from the Tiziano bed (IGSN: IEDS1000R), which marks the position of the proposed GSSP for the base of the Priabonian (Agnini et al., 2011). $^{206}Pb/^{238}U$ dates ranged between 37.792 and 38.341 Ma. The weighted mean age of the youngest five grains is 37.808 ± 0.018/0.022/0.046 Ma (MSWD=1.08), and is mostly supported by CL-imaged zircon tips. However, as with grains from the Canaletto bed, the Tiziano dataset includes both imaged and non-imaged zircon tips (z149 and z1 respectively) that crystallized 100-200 kyr prior to the interpreted eruption age of the tuff, highlighting the role of prolonged growth and/or detrital contamination in generating the observed age distributions. The Bayesian approach of Keller et al. (2018) gave an eruption age of 37.762 ± 0.064/0.065/0.077 Ma. If the oldest, non-reproducible zircon date from this sample is excluded from interpretation as discussed for sample COL12-7248C above, the eruption age becomes 37.780 ± 0.043/0.044/0.061 Ma.

In summary, the weighted mean age of each of the Alano di Piave tuffs is supported by 4-7 reproducible single zircon (or zircon fragment) $^{206}Pb/^{238}U$ dates. Mean ages that include additional data points from each sample are characterized by unacceptably high MSWD values, and are considered to have low probability. Eruption ages determined using the Bayesian approach of Keller et al. (2018) are statistically equivalent to the weighted mean interpretation, but are nominally younger and also less precise. The impact of the choice of interpretive framework for the $^{206}Pb/^{238}U$ data, as well as that of the assumptions underpinning the selection of analyses to be used for each interpretation on the comparison between interpreted U-Pb ages and the astrochronology developed in this study are explored in greater detail in Section 4.5 and Fig. 4.

4.2 Calcimetry results

Dietrich-Fruhling calcimetry results show the same short-term variance and trend as the data from the stable isotope runs of Spofforth et al. (2010), however they did not reproduce a 10% decrease of average wt.% $CaCO_3$ reported in the latter dataset around 60 m, resulting in a large scatter of absolute values for the upper part of the investigated interval (Fig. 2).

4.3 Spectral Analysis and cyclostratigraphy

Interpreted U-Pb data suggest a rather uniform sedimentation rate of the surveyed interval at Alano di Piave. The average sedimentation rate between the level COL12-7248C at 104 m dated at 36.583± 0.046 Ma and the Tiziano Bed at 64 m dated at 37.789± 0.024 Ma is ~ 3.3 cm/kyr, providing a basis for further cyclochronological analysis.

Based on this average sedimentation rate, the MTM analysis of the $\delta^{13}C$ and wt.% $CaCO_3$ records reveals significant spectral densities in the frequency ranges expected for orbital components in the depth domain (Fig. 5). However, the wt.% $CaCO_3$ record, does not show a significant signature of orbital forcing in the frequency range of both short and long eccentricity (Fig. 5). Changes in runoff in a tectonically active area (e.g., Doglioni and Bosellini, 1987; Carminati and Doglioni, 2012) might explain the obliteration of the lower frequency orbital components in the wt.% $CaCO_3$ record, while preserving the precessional signature that works at a time scale too short to be influenced by tectonics.

Gaussian filtering (frequency 0.8 cycle/m – bandwidth 0.24 cycle/m) of the 405 kyr component from the $\delta^{13}C$ records was used to establish a first cyclochronological framework for the Alano di Piave record. Filtered $\delta^{13}C$ data showed ~ 5 long eccentricity cycles resulting in a total duration of ~ 2 Myr for the surveyed segment (Figure 6). The application of a 100 kyr filter, corresponding to ~0.3 cycles/m in the depth domain, to the $\delta^{13}C$ record shows the expected amplitude modulation (AM) of the long eccentricity forcing (Figure 6). This allows establishing the filter signal phasing with respect to the astronomical solution of Laskar et al. (2011 – La2010d). Three intervals of AM maxima were identified, at ca. 70, 85 and 98 m, the youngest and oldest of which correspond to the C17n.1n/C16r boundary and the top of the short C17n.1r reversal, and are in line with the results of Westerhold et al. (2014) who dated this magnetostratigraphic boundary at 37.385 Ma. We, therefore, use this astronomical age to tune our record to long eccentricity cycle maxima 91 to 95 of the La2010d solution (Fig. 6). Below 60m, minimal short eccentricity forcing in the corresponding time interval (Laskar et al., 2011) precludes the detection of 100 kyr cycles, in the $\delta^{13}C$ record. Nonetheless, the sum of the short and long eccentricity periodic components from the $\delta^{13}C$ dataset (the green line in Fig. 6) tracks the weak short eccentricity forcing associated with the 2.4 Myr minimum in the La2010d solution. The latter imposes lows in the $\delta^{13}C$ and $CaCO_3$ records (Figure 6) to be associated with maxima of the 405 kyr forcing. We further test the phasing of the filtered orbital components by applying an EHA to the $\delta^{13}C$ record in order to recognise the frequency modulation (FM) of the eccentricity components (e.g. Laurin et al., 2016; Galeotti et al., 2017). The EHA analysis carried out on the $\delta^{13}C$ record provides a clear identification of the FM of the two components of short eccentricity (E2 and E3 in Fig. S1) for the upper part of the surveyed interval, where nodes of maximal FM are observed in the same stratigraphic intervals where maximal AM occurs in the filtered $\delta^{13}C$ record. Therefore, in spite of a weaker short eccentricity signal in the lower part of the surveyed interval, the documentation of AM and FM in the $\delta^{13}C$ record provides strong evidence for the identification of 405 kyr maxima.

4.4. Paleoceanographic implications

Both filtering of the eccentricity components (AM) and EHA spectrum analysis (FM), show that the $\delta^{13}C$ record neatly tracks the transition from a time interval dominated by the 405 kyr eccentricity, evident between 38.5–37.8 Ma in the EHA of the La2010d astronomical solution of eccentricity, suggesting a strong dependency of the marine carbon cycle on orbital forcing. Such a close coupling between external forcing(s) and the carbon cycle is well known for Quaternary glacial-interglacial changes in ice volume and temperature as well as for older geological intervals (e.g. the Early Oligocene; Palike et al., 2006) characterised by the presence of a sufficiently large ice sheet to impose large feedbacks to the biogeochemical cycle(s) (Zachos and Kump, 2005).

Interestingly, the occurrence of an obliquity-dominated cyclicity in correspondence of the same 2.4 Myr eccentricity minimum in oceanic records (i.e. ODP Sites 1172 and 1052) together with relatively high amounts of ice-rafted debris observed in the Greenland Semodla Site 913 (Eldrett et al., 2007; Tripati et al., 2008) has been suggested to result from the possible influence of ice in high latitude settings (Westerhold et al., 2014), in line with previous suggestions that temperatures were sufficiently low to form ice in the Arctic already from 47–46 Ma ago (Stickley et al., 2009; St. John et al., 2008). The occurrence of a larger obliquity signature across the 2.4 Myr eccentricity node centered between 405 kyr cycle maxima 94 and 95 (see Fig. 6 and Fig. S1) would provide further evidence in favour of this idea. To test this hypothesis, we run a Singular Spectrum Analysis (SSA; windows=30) on the $\delta^{13}C$ record, after tuning it to the La2010d astronomical solution, of two distinct segments within the surveyed stratigraphic interval (Fig. S2). The first segment spans 40m to 70 m, which corresponds to a time interval (~38.5 Ma to ~37.5 Ma) characterised by minimal eccentricity forcing (Laskar et al., 2011). The second segment spans 70m to 104m, which corresponds to a time interval (~37.5 Ma to ~36.5 Ma) characterised by maximal eccentricity forcing. Considering the remarkable orbital control on carbon cycle, one should expect obliquity to have a quantitatively more important signature within the lower segment. However, obliquity frequency components in the $\delta^{13}C$ record have a relative weight higher (~7% of the entire signal variance using an SSA window of length equal to 30) in the 37.5–36.5 Ma time interval than observed in the 38.5–37.5 Ma time interval (~2% of the total signal variance). Gaussian filtering of the tuned $\delta^{13}C$ record provides very similar results. The lower segment – characterised by weak short eccentricity cycles, thus enhanced 405 kyr cycles – shows a weaker obliquity signal compared to the higher segment, which is also characterised by strong short eccentricity. This result is largely expected for eccentricity. In fact, according to the filter of the long-term eccentricity modulation (Zeebe, 2017) a minimal modulation node is centred at 38.1 Ma while maximal modulation occurs at 36.7 Ma. However, the 41 kyr filter of the $\delta^{13}C$ does not follow the long-term modulation of obliquity (Fig. 7). Moreover, this result is at odds with previous suggestion of a stronger obliquity signature across the 2.4 Myr node at 38.1 Ma and, in general, during time intervals characterised by lower eccentricity forcing. The absence of prominent obliquity cycles in the 38.5–37.5 Ma interval could be explained with the low latitude paleogeographic position of the Alano Section. However, this does not explain why obliquity becomes more prominent in a time interval (37.5–36.5 Ma) characterised by higher short eccentricity forcing. On the other hand, the effect of obliquity forcing is markedly confined to high latitude settings, which suggests that the obliquity cycles recorded at Alano track a high latitude signal, which is then transferred through feedback at a supra-regional scale. Diagenesis, would be an alternative explanation. Yet, a differential preservation effect tracking obliquity cycles would not be independent from obliquity forcing in any case. Because the signal is not univocal at the global scale the different response at different locations and water depths could be related to changes in the organization of intermediate to deep-water circulation caused by the response of high latitude settings to orbital forcing. Compared to above mentioned sites, however, the Alano di Piave record is characterised by the same phase relation of isotopes vs. carbonate content with low $\delta^{13}C$ corresponding to low wt%$CaCO_3$ over the 38.5Ma–36.5. Such a phase relationship is suggestive of an Atlantic-type (high carbonate during interglacials) mode of carbonate stratigraphy (Moore Jr. et al., 1982; Dunn, 1982), which would shift to a Pacific-type (high carbonate during glacials) at about 36 Ma according to Westerhold et al. (2014).

4.5. Comparison of astrochronology and radio-isotopic results

A comparison between U-Pb age constraints and the astrochronology derived in this study confirms that the tuning of the Alano record to the 405 kyr eccentricity signal is broadly correct (Fig. 8). The

405-kyr eccentricity cycle has remained relatively stable during the geologica time with an estimated uncertainty of ~500kyr at 250 Ma. For the time interval under consideration the maximum estimated uncertainty is ~30 kyr (Laskar et al., 2004). While we provide astronomical ages according to the most recent astronomical solution of Laskar et al (2010b), this uncertainty is taken into account for comparison with interpreted U-Pb data, as shown in Figure 4. The agreement between the $^{206}Pb/^{238}U$ and astronomically tuned age of individual crystal-rich tuffs at the 2σ level is dependent on the choice of interpretive framework for U-Pb data, and the uncertainties assigned to the tuning. It should be noted that when it comes to the amount of time elapsed between the deposition of consecutive volcanic beds, except for the COL12-7248C – Canaletto pair, both dating methods give results that are within 20 kyr of each other (i.e. Canaletto – COL12-5229C = 380/400 kyr, COL12-5229 – Tiziano = 610/620 kyr) which suggests that precession-level tuning is correct between 64 – 96 m. For the COL12-7248C – Canaletto pair, the astronomically tuned duration (240 kyr) exceeds that derived from U-Pb dating by 80 – 100 kyr depending on whether the zircon data are interpreted in terms of weighted means, or using the Bayesian approach of Keller et al. (2018), respectively.

Interpretation of the zircon U-Pb data in terms of acceptable-MSWD weighted mean dates results in small discrepancies relative to astronomical age of each crystal-rich tuff. These discrepancies are statistically significant given the total 2σ U-Pb age uncertainties (including ^{238}U decay constant and isotopic tracer calibration uncertainties), and the 10 kyr (half a precession cycle) uncertainty assigned to the astronomical ages. The interpreted zircon $^{206}Pb/^{238}U$ age of a volcanic tuff, and its associated uncertainty, can vary to some extent based on the number of grains included in each mean age, as well as other measured or assumed parameters that are involved in age calculations, such as the initial Th/U ratio of the magma from which the zircons crystallised (hereafter Th/U_{magma}). The impact of these factors on the discrepancy between our U-Pb dates and astronomically tuned ages is explored in Fig. 4. For each tuff, all alternative interpretations of the $^{206}Pb/^{238}U$ data considered here are statistically equivalent at the 2σ level. However, the size of the inter-method discrepancies considered here is such that they can be cancelled out by even minute variations in nominal $^{206}Pb/^{238}U$ age and uncertainty. The inter-method discrepancy decreases slightly when weighted mean dates based on fewer grains than our preferred interpretation are considered, as the nominal age decreases and the age uncertainty increases for mean ages based on fewer analyses. In fact, the youngest date from the Canaletto bed is statistically equivalent to the respective astronomically tuned age (Fig. 4). However, given that there is no detectable geological scatter affecting the dates included in our preferred U-Pb data interpretation at the resolution of their 2σ uncertainties (see also Section 4.1) we see no compelling reason to subjectively exclude any of the data encompassed therein and rely on a sole determination that has by definition has not been reproduced and could represent that sampling of a population. Given that all $^{206}Pb/^{238}U$ dates from this study are older than the astronomically tuned ages of the respective volcanic beds, the observed discrepancy is likely to be systematic. One potential factor is the assumed Th/U_{magma} ratio, which impacts age interpretation as zircons incorporate U preferentially over Th, thus creating an initial disequilibrium which must be accounted for, particularly for relatively young samples. The interpreted age of a volcanic tuff decreases with decreasing Th/U_{magma}, as illustrated in Fig. 4, however agreement between our U-Pb dates and astronomical age estimates would require Th/U_{magma} values at or below 1, which is unrealistic if we assume that magma composition would approach the average continental crust Th/U ratio of ~ 5 (Paul et al., 2003). A systematic offset of the U-Pb dataset resulting from the ^{238}U decay constant, or the correction applied to account for laboratory Pb blank is unlikely, because this study uses the same systematic parameters as in similar Cenozoic studies (e.g. Sahy et al., 2017) found to be in good agreement with the astronomically tuned Oligocene time scale of Pälike et al. (2006).

Conversely, eruption ages obtained using the Bayesian approach of Keller et al. (2018) result are in agreement with astronomical dates for three out of the four dated tuffs. The exception is tuff COL12-7248C, where the eruption age is nominally 120 kyr older than the astronomical age (for comparison, the offset between the acceptable-MSWD weighted mean and the astronomical age is

160 kyr). However, the Tiziano tuff presents an interesting test case for the Bayesian approach. When all measured $^{206}Pb/^{238}U$ dates are included in the calculated eruption age, the offset between this and the astronomical age is 52 ± 77 kyr (i.e. the two dates are statistically equivalent at the 2σ level when all analytical and systematic uncertainties associated with U-Pb dating and the 10 kyr uncertainty assigned to the astronomical tuning are taken into account). If the oldest non-reproducible $^{206}Pb/^{238}U$ date from the Tiziano tuff is excluded from the interpretation, the offset between the eruption age and the astronomical age becomes 70 ± 61 kyr, and in order to reach statistical agreement between the two dating methods the uncertainty of the astronomically tuned age must be increased from 10 to 40 kyr, or roughly 0.1% of the nominal age. Although the U-Pb dataset presented here is modest, with only four tuffs analysed, the results suggest that the Bayesian approach of Keller et al. (2018) is likely to outperform conventional weighted mean interpretations in terms of accuracy (assuming our astronomical tuning of the Alano di Piave section is correct) when the underlying assumptions are valid. However, this requires that: (i) the measured $^{206}Pb/^{238}U$ dates must accurately capture the range of crystallization ages present in the sample and (ii) the dataset must be free of dates biased towards younger or older values through open-system behaviour, contamination or the inclusion of unidentified xenocrists. The validity of these assumptions is difficult to assess for relatively low-n datasets (e.g. 10 – 11 zircons analysed per sample in this study) for which both weighed mean and Bayesian interpretations should be used with consideration.

4.6. Astrochronology of the Bartonian-Priabonian transition

Using the precessional component from the $CaCO_3$% and $\delta^{13}C$ records allows establishing an accurate floating cyclochronology across the Bartonian–Priabonian transition (Fig. 9). Cycle counting allows us to determine the duration of individual magnetochrons (Table S2) and the time relationship between biostratigraphic and magnetostratigraphic zonal boundaries.

Independently of the concept that will be used to define the base Priabonian GSSP level, this exercise will facilitate its global correlation based on magnetostratigraphy and standard calcareous plankton biostratigraphy, which are available for the Alano di Piave section (Agnini et al., 2011). We use the base of the Tiziano Bed, which has been proposed by Agnini et al. (2011) to define the GSSP, as a time zero level assigning negative values for events preceding it and positive values for events following it (Fig. 9). The estimated duration of magnetochrons well match the results recently obtained by Westerhold et al. (2014), although presenting minor differences (Table 2).
Combined precession and short eccentricity cycles counting allows to estimate that the lowest occurrence of *Globigerinatheka semiinvoluta* occurs 142 kyr after the deposition of the Tiziano Bed; the acme of *Cribrocentrum erbae* and the rare first occurrence of *Chiasmolithus oamaruensis* occur 20 kyr and 22 kyr before the deposition of the Tiziano Bed, respectively; the highest occurrences of the genus *Morozovelloides* and of large acarininids precede the deposition of the Tiziano Bed by 170 kyr and 173 kyr, respectively (Fig. 9).

5. Conclusions

The spectral analysis of the proposed Priabonian GSSP section of the Alano di Piave has revealed periodic components that can be ascribed to astronomical forcing. Filtering of these components has allowed establishing a floating astrochronology and to tune the periodic components to the astronomical solution of Laskar et al. (2011) (La2010d). The tuning is broadly in agreement with zircon $^{206}Pb/^{238}U$ dates obtained on four volcanic tuffs intercalated in the record, although statistical agreement between these and the astronomical age of each tuff is subject to the uncertainty assigned to both the astronomically tuned record and U-Pb geochronology.
Cycle counting allowed us to establish a time relationship between individual bio- and magnetostratigraphic events across the Bartonian-Priabonian transition. This result, independently of the concept that will be adopted by the Submcommision on Paleogene Stratigraphy for the

definition of the base Priabonian GSSP, will facilitate its correlation on a global scale by the of magnetostratigraphy and standard calcareous plankton biostratigraphy.

Short- and long eccentricity cycles dominate the $\delta^{13}C$ record from the Alano di Piave succession providing evidence for a strong dependency of carbon cycle on astronomical forcing in the surveyed time interval. However, comparison with carbon isotope profiles from Atlantic and Pacific oceanic sites reveals differences in the response to astronomical forcing, which could be related to water mass organization.

Acknowledgements

This research benefited from funds provided by MIUR-PRIN grant 2010X3PP8J_005 to SG and 2010X3PP8J_003 to DR, by a PhD Grant of the Italian Minister for Research to FF and ERC Consolidator Grant 617462 “EarthSequencing” to HP. DS received support through the European Community’s Seventh Framework Programme (FP7/2007-2013) under grant agreement n° 215458. We thank Jörn Wotzlaw and an anonymous reviewer for their constructive comments on our manuscript.

References

Agnini, C., Fornaciari, E., Giusberti, L., Grandesso, P., Lanci, L., Luciani, V., Muttoni, G., Palike, H., Rio, D., Spofforth, D.J.A., Stefani, C., 2011. Integrated biomagnetostratigraphy of the Alano section (NE Italy): A proposal for defining the middle-late Eocene boundary. Geological Society of America Bulletin 123, 841–872. https://doi.org/10.1130/B30158.1.

Agnini C., Backman J., Fornaciari E., Galeotti S., Giusberti L., Grandesso P., Lanci L., Monechi S., Muttoni G., Pälike H., Pampaloni M.L., Pignatti J., Premoli Silva I., Raffi I., Rio D., Rook L., Stefani C., 2014. The Alano section: the candidate GSSP for the Priabonian Stage.

STRATI 2013 First International Congress on Stratigraphy. At the Cutting Edge of Stratigraphy. Springer Geology, Berlin, 55-59. https://doi.org/10.1007/978-3-319-04364-7_11.

Beccaluva L., Bianchini G., Bonadiman C., Coltorti C., Milani L., Salvini L., Siena F., Tassinari R., 2007. Intraplate lithospheric and sublithospheric components in the Adriatic domain: Nephelinite to tholeiite magma generation in the Paleogene Veneto volcanic province, southern Alps. In: Beccaluva, L., Bianchini, G., and Wilson, M., (eds.), 2007, Cenozoic Volcanism in the Mediterranean Area: Geological Society of America Special Paper 418, 335 p. https://doi.org/10.1130/2007.2418(07)

Bowring S.A., Schmitz, M.D., 2003. High-Precision U-Pb Zircon Geochronology and the Stratigraphic Record. Reviews in Mineralogy and Geochemistry 53, 305–326. https://doi.org/10.2113/0530305

Bowring, J.F., McLean, N.M., Bowring, S.A., 2011. Engineering cyber infrastructure for U-Pb geochronology: Tripoli and U-Pb_Redux. Geochemistry, Geophysics, Geosystems 12. https://doi.org/10.1029/2010GC003479.

Carminati, E., Doglioni, C., 2012. Alps vs. Apennines: The paradigm of a tectonically asymmetric Earth. Earth-Science Reviews 112, 67–96. https://doi.org/10.1016/j.earscirev.2012.02.004.

Condon, D.J., Schoene, B., McLean, N.M., Bowring, S.A., Parrish, R.R., 2015. Metrology and traceability of U–Pb isotope dilution geochronology (EARTHTIME Tracer Calibration Part I). Geochimica et Cosmochimica Acta 164, 464–480. https://doi.org/10.1016/j.gca.2015.05.026.

Doglioni, C., Bosellini, A., 1987. Eoalpine and mesoalpine tectonics in the Southern Alps. Geologische Rundschau, 76, 735-754. doi: 10.1007/BF01821061.

Dunn, D. A., 1982. Change from "Atlantic-type" to "Pacific-type" carbonate stratigraphy in the middle Pliocene Equatorial Pacific Ocean, Mar. Geol., 50, 41–59, doi:10.1016/0025-3227(82)90060-3.

Eldrett, J.S., Harding, I.C., Wilson, P.A., Butler, E., Roberts, A.P., 2007. Continental ice in Greenland during the Eocene and Oligocene. Nature 446, 176–179. https://doi.org/10.1038/nature05591.

Galeotti, S., Moretti, M., Sabatino, N., Sprovieri, M., Ceccatelli, M., Francescone, F., Lanci, L., Lauretano, V., Monechi, S., 2017. Cyclochronology of the Early Eocene carbon isotope record from a composite Contessa Road-Bottaccione section (Gubbio, central Italy). Newsletters on Stratigraphy 50, 231–244. https://doi.org/10.1127/nos/2017/0347.

Hiess, J., Condon, D.J., McLean, N., Noble, S.R., 2012. 238U/235U Systematics in Terrestrial Uranium-Bearing Minerals. Science 335, 1610–1614. https://doi.org/10.1126/science.1215507.

C.B. Keller, P. Boehnke, B. Schoene, 2017. Temporal variation in relative zircon abundance throughout Earth history. Geochem. Perspect. Lett. 3, 179–189. https://doi.org/10.7185/geochemlet.1721

Keller, C.B., Schoene, B., Samperton, K.M., 2018. A stochastic sampling approach to zircon eruption age interpretation. Geochem. Perspect. Lett. 8, 31–35. https://doi.org/10.7185/geochemlet.1826

Jaffey, A.H., Flynn, K.F., Glendenin, L.E., Bentley, W.C., Essling, A.M., 1971. Precision Measurement of Half-Lives and Specific Activities of 235U and 238U. Physical Review C 4, 1889–1906. https://doi.org/10.1103/PhysRevC.4.1889.

Laskar, J., Robutel, P., Joutel, F., Gastineau, M., Correia, A.C.M., Levrard, B., 2004. A long- term numerical solution for the insolation quantities of the Earth. Astronomy and Astrophysics 428, 261–285.

Laskar, J., Fienga, A., Gastineau, M., Manche, H., 2011. La2010: a new orbital solution for the long-term motion of the Earth. Astronomy & Astrophysics 532, A89. https://doi.org/10.1051/0004-6361/201116836.

Laurin, J., Meyers, S.R., Galeotti, S., Lanci, L., 2016. Frequency modulation reveals the phasing of orbital eccentricity during Cretaceous Oceanic Anoxic Event II and the Eocene hyperthermals. Earth and Planetary Science Letters 442, 143–156. https://doi.org/10.1016/j.epsl.2016.02.047.

Mattinson, J.M., 2005. Zircon U–Pb chemical abrasion ("CA-TIMS") method: Combined annealing and multi-step partial dissolution analysis for improved precision and accuracy of zircon ages. Chemical Geology 220, 47–66. https://doi.org/10.1016/j.chemgeo.2005.03.011.

McLean, N.M., Bowring, J.F., Bowring, S.A., 2011. An algorithm for U-Pb isotope dilution data reduction and uncertainty propagation. Geochemistry, Geophysics, Geosystems 12. https://doi.org/10.1029/2010GC003478.McLean, N. M., Bowring, J. F., and Bowring, S. A., 2011, An algorithm for U-Pb isotope dilution data reduction and uncertainty propagation: Geochem. Geophys. Geosyst., v. 12, doi: 10.1029/2010GC003478.

Moore Jr., T. C., Pisias, N. G., Dunn, D. A., 1982. Carbonate time series of the Quaternary and Late Miocene sediments in the Pacific Ocean: A spectral comparison, Mar. Geol., 46, 217–233.

Meyers, S.R., 2014. astrochron: An R Package for Astrochronology. http://cran.r-project.org/package=astrochron

Pälike, H., Norris, R.D., Herrle, J.O., Wilson, P.A., Coxall, H.K., Lear, C.H., Shackleton, N.J., Tripati, A.K., Wade, B.S., 2006. The Heartbeat of the Oligocene Climate System. Science 314, 1894–1898. https://doi.org/10.1126/science.1133822.

Paul, D., White, W.M., Turcotte, D.L., 2003. Constraints on the 232Th/ 238U ratio (κ) of the continental crust. Geochemistry, Geophysics, Geosystems 4. https://doi.org/10.1029/2002GC000497.

Sageman, B.B., Singer, B.S., Meyers, S.R., Siewert, S.E., Walaszczyk, I., Condon, D.J., Jicha, B.R., Obradovich, J.D., Sawyer, D.A., 2014. Integrating 40Ar/39Ar, U-Pb, and astronomical clocks in the Cretaceous Niobrara Formation, Western Interior Basin, USA. Geological Society of America Bulletin 126, 956–973. https://doi.org/10.1130/B30929.1.

Sahy, D., Condon, D.J., Terry, D.O., Fischer, A.U., Kuiper, K.F., 2015. Synchronizing terrestrial and marine records of environmental change across the Eocene–Oligocene transition. Earth and Planetary Science Letters 427, 171–182. https://doi.org/10.1016/j.epsl.2015.06.057.

Sahy, D., Condon, D.J., Hilgen, F.J., Kuiper, K.F., 2017. Reducing Disparity in Radio-Isotopic and Astrochronology-Based Time Scales of the Late Eocene and Oligocene: U-Pb Dating of the Paleogene Time Scale. Paleoceanography 32, 1018–1035. https://doi.org/10.1002/2017PA003197.

Samperton, K.M. , Bell, E.A., Barboni, M, Keller, C.B., Schoene, B., 2017. Zircon age-temperature-compositional spectra in plutonic rocks. Geology 45,. 983–986. https://doi.org/10.1130/G38645.1

Schoene, B., 2014. U–Th–Pb Geochronology, in: Treatise on Geochemistry. Elsevier, pp. 341–378. https://doi.org/10.1016/B978-0-08-095975-7.00310-7.

Sciunnach, D., Borsato, A., 1994. Plagioclase-arenites in the Molveno Lake area (Trento): record of an Eocene volcanic arc. Studi Trentini di Scienze Naturali, Acta Geologica 69 (1994), 81-92.

Spofforth, D.J.A., Agnini, C., Pälike, H., Rio, D., Fornaciari, E., Giusberti, L., Luciani, V., Lanci, L., Muttoni, G., 2010. Organic carbon burial following the middle Eocene climatic optimum in the central-western Tethys. Paleoceanography 25, 3210. https://doi.org/10.1029/2009PA001738.

St. John, K., 2008. Cenozoic ice-rafting history of the central Arctic Ocean: Terrigenous sands on the Lomonosov Ridge. Paleoceanography 23. https://doi.org/10.1029/2007PA001483.

Stickley, C.E., St John, K., Koç, N., Jordan, R.W., Passchier, S., Pearce, R.B., Kearns, L.E., 2009. Evidence for middle Eocene Arctic sea ice from diatoms and ice-rafted debris. Nature 460, 376–379. https://doi.org/10.1038/nature08163.

Tripati, A.K., Eagle, R.A., Morton, A., Dowdeswell, J.A., Atkinson, K.L., Bahé, Y., Dawber, C.F., Khadun, E., Shaw, R.M.H., Shorttle, O., Thanabalasundaram, L., 2008. Evidence for glaciation in the Northern Hemisphere back to 44 Ma from ice-rafted debris in the Greenland Sea. Earth and Planetary Science Letters 265, 112–122. https://doi.org/10.1016/j.epsl.2007.09.045.

Watson, E.B., 1996. Dissolution, growth and survival of zircons during crustal fusion: kinetic principles, geological models and implications for isotopic inheritance. Trans. R. Soc. Edinb. Earth Sci. 87, 43–56. https://doi.org/10.1017/S0263593300006465.

Wendt, I., Carl, C., 1991. The statistical distribution of the mean squared weighted deviation. Chemical Geology: Isotope Geoscience section 86, 275–285. https://doi.org/10.1016/0168-9622(91)90010-T.

Westerhold, T., Röhl, U., Pälike, H., Wilkens, R., Wilson, P.A., Acton, G., 2014. Orbitally tuned timescale and astronomical forcing in the middle Eocene to early Oligocene. Climate of the Past 10, 955–973. https://doi.org/10.5194/cp-10-955-2014.

Wotzlaw, J.F., Hüsing, S.K., Hilgen, F.J., Schaltegger, U., 2014. High-precision zircon U–Pb geochronology of astronomically dated volcanic ash beds from the Mediterranean Miocene. Earth and Planetary Science Letters 407, 19–34. https://doi.org/10.1016/j.epsl.2014.09.025.

Zachos, J., Kump, L., 2005. Carbon cycle feedbacks and the initiation of Antarctic glaciation in the earliest Oligocene. Global and Planetary Change 47, 51–66. https://doi.org/10.1016/j.gloplacha.2005.01.001.

Zeebe, R.E., 2017. Numerical Solutions for the Orbital Motion of the Solar System over the Past 100 Myr: Limits and New Results. The Astronomical Journal 154, 193. https://doi.org/10.3847/1538-3881/aa8cce.

Figure and table captions

Table 1. Summary of inferred radioisotopic and astrochonological ages of selected volcaniclastic layers from the Alano di Piave section. † - $^{206}Pb/^{236}U$ low MSWD weighted mean age, * - eruption age calculated using the Bayesian approach of Keller et al. (2018), ** - eruption age calculated using the Bayesian approach of Keller et al. (2018) after excluding the oldest non-reproducible zircon date from a given tuff.

Figure 1. Location map of the study area with indication of the Alano section. The best access to the section (dashed line) is also reported. Modified from Agnini et al. (2011).

Figure 2. wt.%$CaCO_3$ and $\delta^{13}C$ records of the Alano di Piave section against the litho-, bio-, and magnetostratigraphy of Agnini et al. (2011). The $\delta^{13}C$ and the wt.%$CaCO_3$ records are from Spofforth et al. (2010). The red line represents replicate analysis of the wt.%$CaCO_3$ record. Volcaniclastic layers analysed for the radio-isotopic age assessment (from top to bottom, COL12-7248, Canaletto, COL12-5229C and Tiziano) are marked in red.

Figure 3. Ranked plot of the results of single-grain $^{206}Pb/^{238}U$, along with conventional, transmitted light and SEM CL images of each analysed grain or grain fragment. From left to right, the zircon images are ordered ascending by age, and match the order in which the data are plotted. The height of each rectangle corresponds to the 2σ analytical uncertainty of the respective date. Dark (light) grey bars represent the analytical (total) uncertainty of the preferred weighted mean for each sample. Analysed CL-imaged grain fragments are marked by a white circle, or identified as A and B where two fragments from the same crystal were analysed. Grain IDs match those in Supplementary Table S1. * - indicates Bayesian eruption ages derived using the

approach of Keller et al. (2018); ** - indicates Bayesian eruption ages derived after excluding the oldest non-reproducible zircon data from a given sample.

Figure 4. Analysis of the impact of U-Pb data interpretation on the comparison between the $^{206}Pb/^{238}U$ and astronomically tuned age of the volcanic tuffs from Alano di Piave. N – number of analyses included in each weighted mean age. MSWD – Mean square of the weighted deviates. Closed/open symbols represent interpretations characterised by MSWD values below/above the acceptable maximum value for a given population size. For each parameter, i.e. MSWD, age of the tuff and Δt and for each N value we plot three options based on Th/U_{magma} values of 1.0 ± 0.5 (lightest shade), 1.9 ± 0.5 (mid-tone) and 2.8 ± 0.5 (darkest shade), of which the latter matches the interpretation given in Section 4.1. The corresponding eruption ages determined using the Bayesian approach of Keller et al. (2018) are plotted in red for each tuff, where (*) indicates that the entire U-Pb dataset for a given sample was used, and (**) indicates exclusion of the oldest non-reproducible date. Input data for Bayesian modelling was corrected using Th/U_{magma} = 2.8 ± 0.5. Data plotted with 2σ analytical uncertainties in Age plot, and 2σ analytical and systematic uncertainties in Δt plot.

Figure 5. Results of the MTM spectral analyses carried out on the wt.% $CaCO_3$ (upper panel) and $\delta^{13}C$ (lower panel) records. The 99%, 95% and 90% confidence levels are reported. Based on the results of the radio-isotopic dating and average sedimentation rate of the studied interval, the expected position of the long (red band) and short (blue band) eccentricity components and precession (green band), is indicated.

Figure 6. Results of the gaussian filtering of the long-eccentricity (blue line) and short eccentricity (green line) components from the $\delta^{13}C$ record across the 40-103 m interval at Alano di Piave. The red line represents the sum of the filtered long- and short-eccentricity components against the $\delta^{13}C$ record from the interval spanning 43-104 m above the base of the section at Alano di Piave. Note the modulation of the filtered signal by the long eccentricity component above ~65 m, and the proposed tuning to the eccentricity solution of Laskar et al. (2011) (La2010d).

Based on tuning, long eccentricity maxima are numbered on corresponding lows of the $\delta^{13}C$ record.

Figure 7. Results of the gaussian filtering of the obliquity (red line), short-eccentricity (green line) and long eccentricity (blu line) components from the tuned $\delta^{13}C$ record of the surveyed interval at Alano di Piave. Results are compared to the La2010d astronomical solution (Laskar et al., 2011) and the long-term amplitude modulation (AM) of obliquity and eccentricity (Zeebe, 2017).

Figure 8. Age depth plot of the Alano di Piave section based on the obtained astrochronology. The position of the radio-isotopically dated samples relative to the inferred astrochronological age is reported. The green area represents the maximum error of the astronomical solution for the time interval under consideration (Laskar et al., 2004).

Figure 9. Floating cyclochronology obtained from the spectral analysis and filtering of the precessional and short eccentricity components in the $\delta^{13}C$ and wt.% $CaCO_3$ records across the Bartonian-Priabonian boundary transition. Cycle counting allows defining the duration of individual magnetochrons, as reported in Table 1, and the time relationship between main calcareous plankton biomarkers.

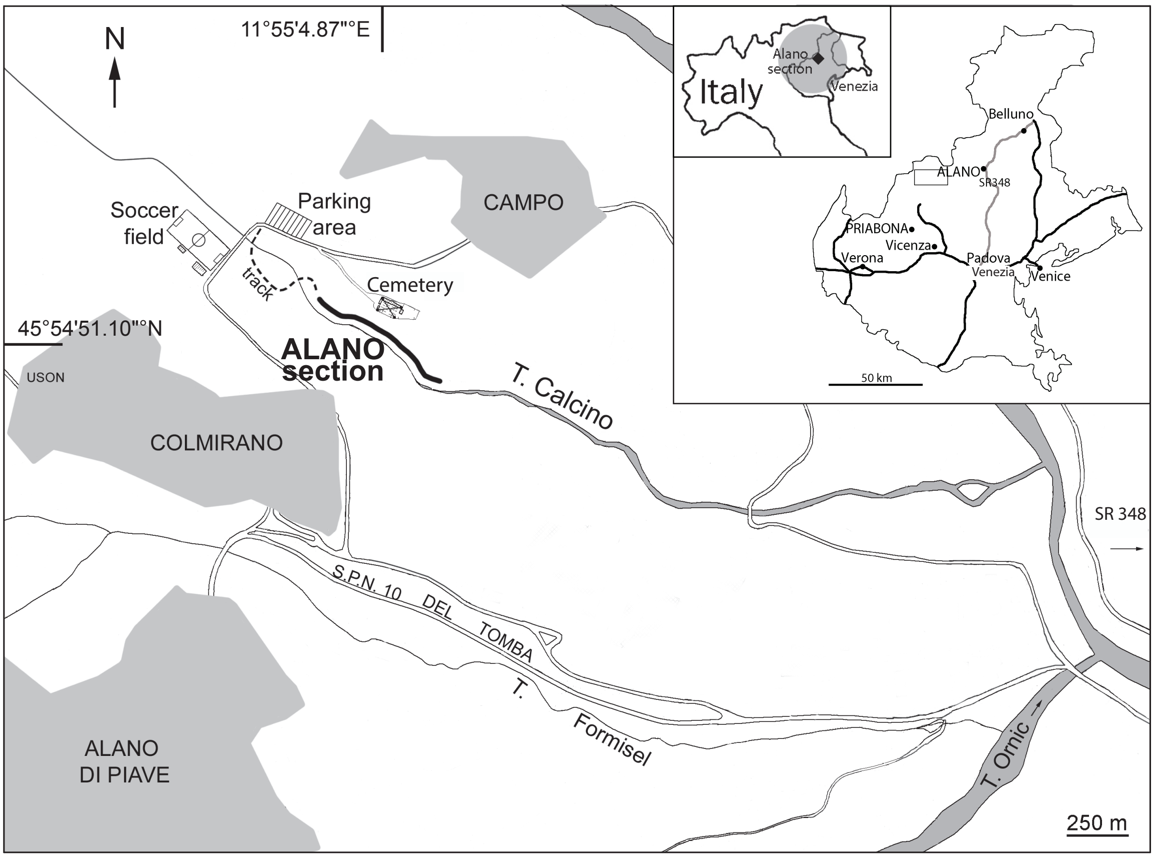

N
11°55'4.87"°E
45°54'51.10"°N
USON
Soccer field
Parking area
CAMPO
track
Cemetery
ALANO section
T. Calcino
COLMIRANO
S.P.N. 10 DEL TOMBA
T. Formisel
ALANO DI PIAVE
T. Ornic
SR 348
250 m
Italy
Alano section
Venezia
Belluno
ALANO
SR348
PRIABONA
Vicenza
Verona
Padova
Venezia
Venice
50 km

Figure 1

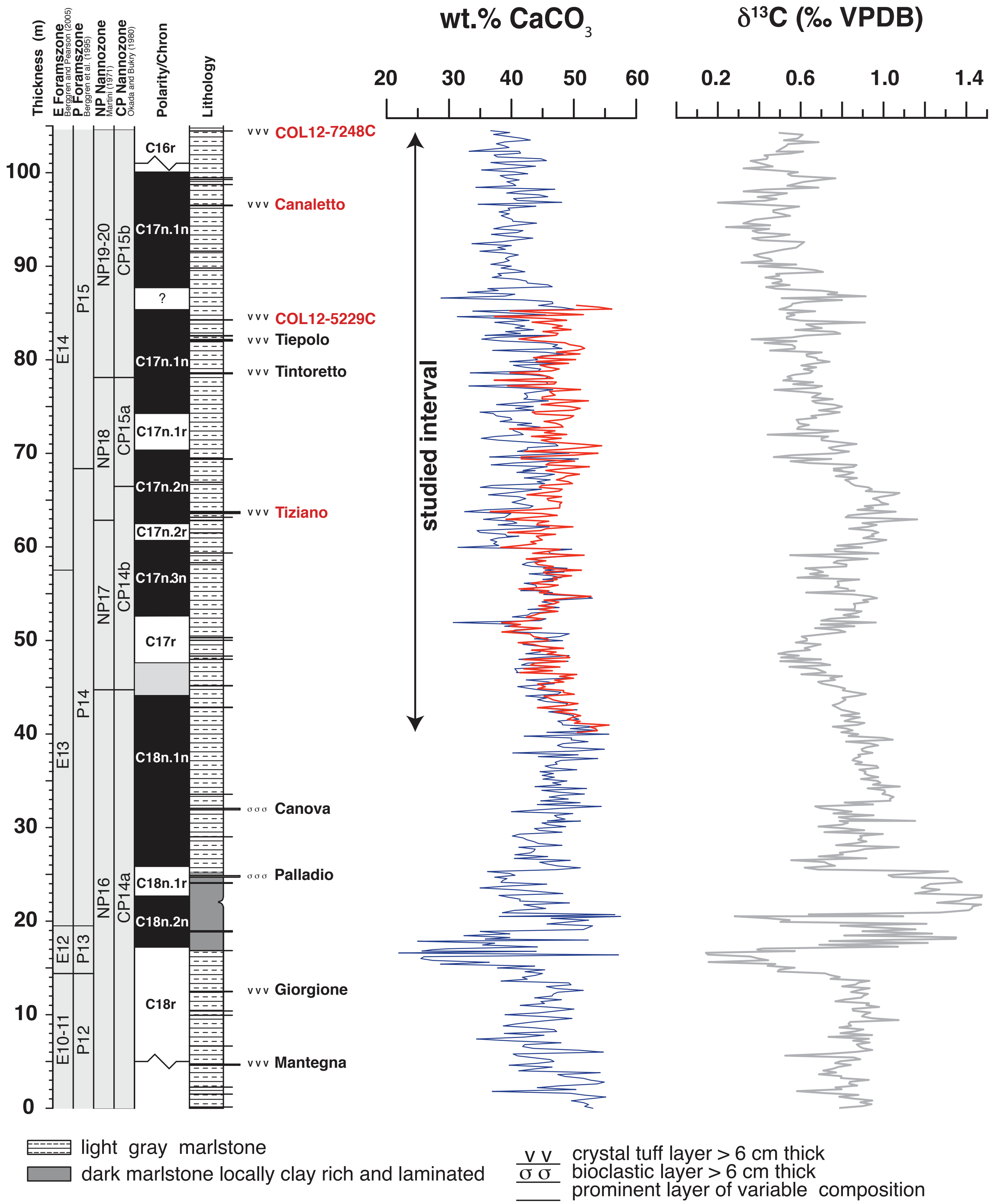

Thickness (m)
E Foramszone
Berggren and Pearson (2005)
P Foramszone
Berggren et al. (1995)
NP Nannozone
Martini (1971)
CP Nannozone
Okada and Bukry (1980)
Polarity/Chron
Lithology
wt.% $CaCO_3$
$\delta^{13}C$ (‰ VPDB)
20 30 40 50 60
0.2 0.6 1.0 1.4
0 10 20 30 40 50 60 70 80 90 100
E10-11
E12
E13
E14
P12
P13
P14
P15
NP16
NP17
NP18
NP19-20
CP14a
CP14b
CP15a
CP15b
C16r
C17n.1n
?
C17n.1n
C17n.1r
C17n.2n
C17n.2r
C17n.3n
C17r
C18n.1n
C18n.1r
C18n.2n
C18r
COL12-7248C
Canaletto
COL12-5229C
Tiepolo
Tintoretto
Tiziano
Canova
Palladio
Giorgione
Mantegna
studied interval
light gray marlstone
dark marlstone locally clay rich and laminated
v v crystal tuff layer > 6 cm thick
σ σ bioclastic layer > 6 cm thick
prominent layer of variable composition

Figure 2

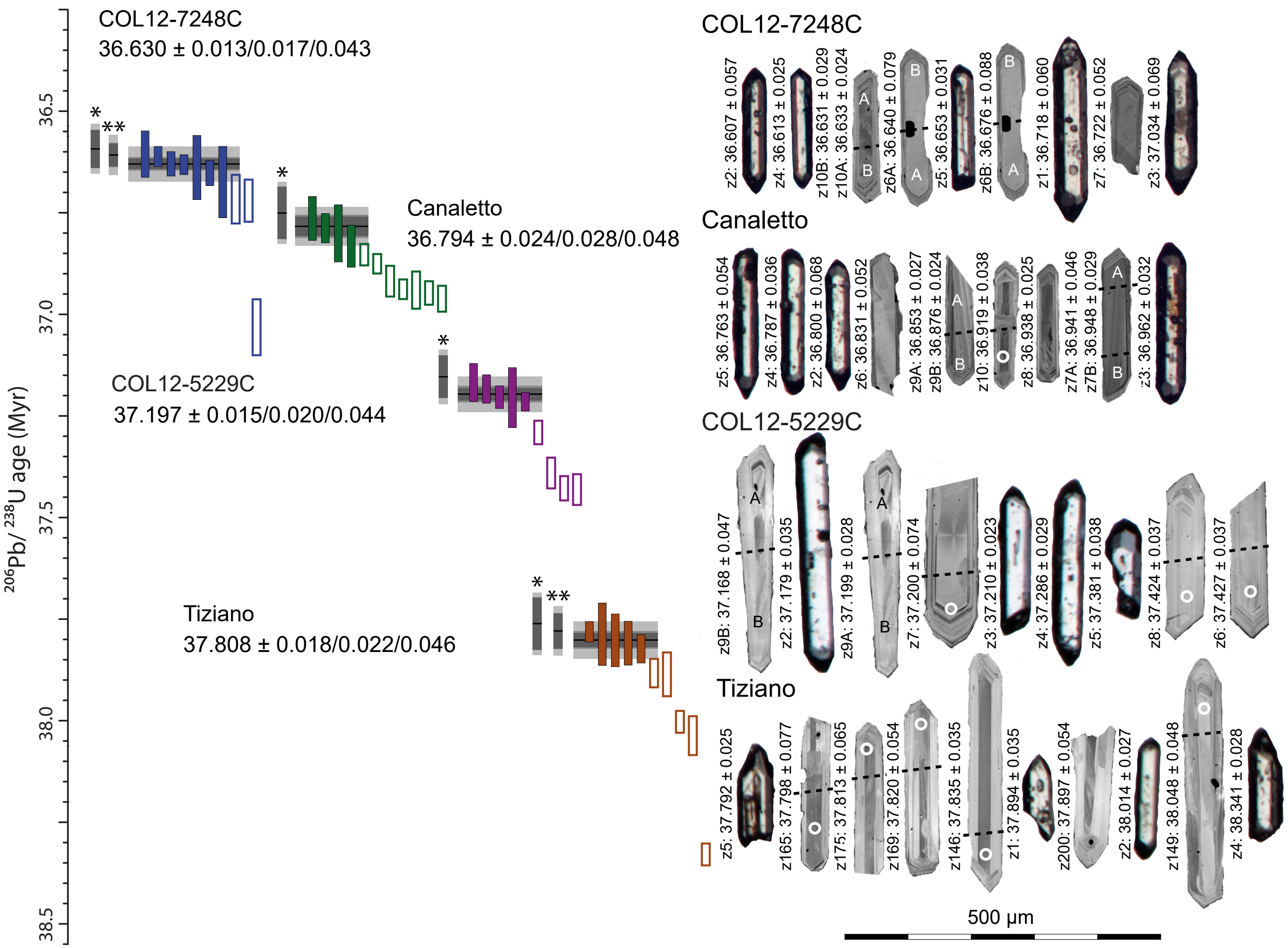

COL12-7248C
36.630 ± 0.013/0.017/0.043
Canaletto
36.794 ± 0.024/0.028/0.048
COL12-5229C
37.197 ± 0.015/0.020/0.044
Tiziano
37.808 ± 0.018/0.022/0.046
206Pb/238U age (Myr)
36.5
37.0
37.5
38.0
38.5
z2: 36.607 ± 0.057
z4: 36.613 ± 0.025
z10B: 36.631 ± 0.029
z10A: 36.633 ± 0.024
z6A: 36.640 ± 0.079
z5: 36.653 ± 0.031
z6B: 36.676 ± 0.088
z1: 36.718 ± 0.060
z7: 36.722 ± 0.052
z3: 37.034 ± 0.069
z5: 36.763 ± 0.054
z4: 36.787 ± 0.036
z2: 36.800 ± 0.068
z6: 36.831 ± 0.052
z9A: 36.853 ± 0.027
z9B: 36.876 ± 0.024
z10: 36.919 ± 0.038
z8: 36.938 ± 0.025
z7A: 36.941 ± 0.046
z7B: 36.948 ± 0.029
z3: 36.962 ± 0.032
z9B: 37.168 ± 0.047
z2: 37.179 ± 0.035
z9A: 37.199 ± 0.028
z7: 37.200 ± 0.074
z3: 37.210 ± 0.023
z4: 37.286 ± 0.029
z5: 37.381 ± 0.038
z8: 37.424 ± 0.037
z6: 37.427 ± 0.037
z5: 37.792 ± 0.025
z165: 37.798 ± 0.077
z175: 37.813 ± 0.065
z169: 37.820 ± 0.054
z146: 37.835 ± 0.035
z1: 37.894 ± 0.035
z200: 37.897 ± 0.054
z2: 38.014 ± 0.027
z149: 38.048 ± 0.048
z4: 38.341 ± 0.028
500 µm

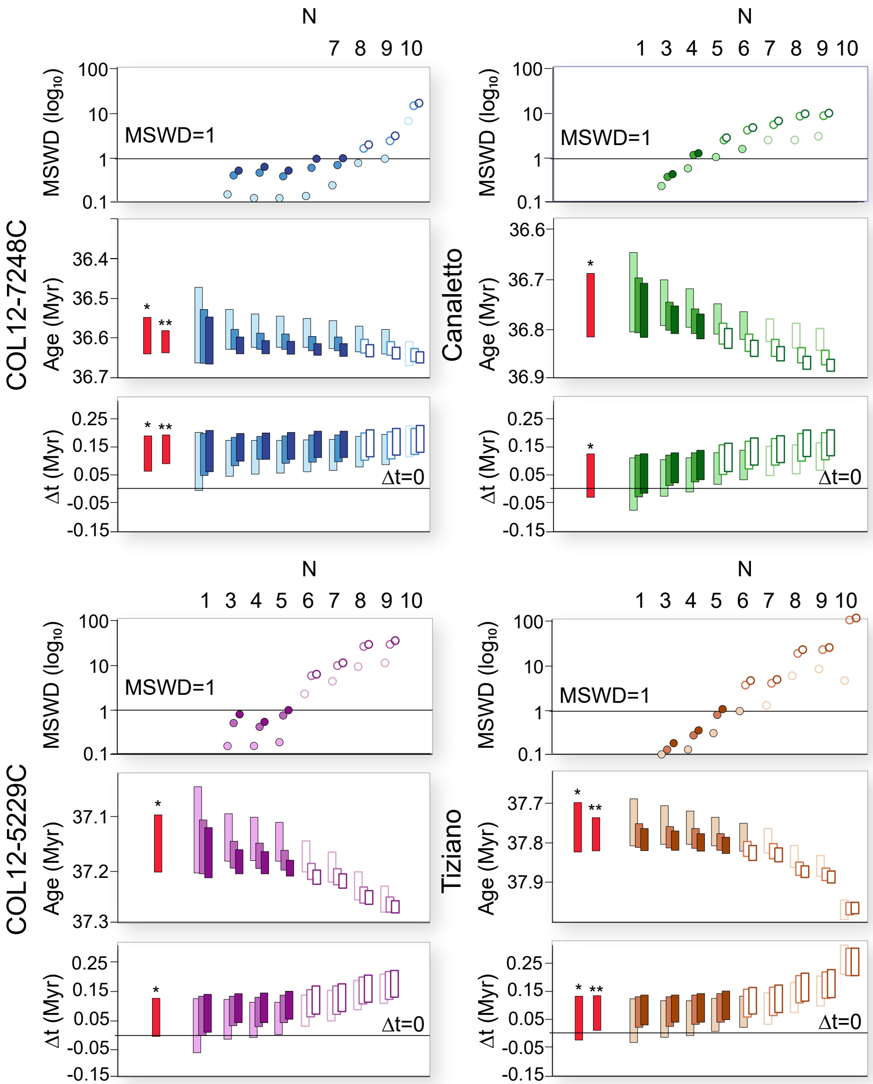
COL12-7248C
Canaletto
COL12-5229C
Tiziano
N
1 3 4 5 6 7 8 9 10
MSWD (log10)
MSWD=1
Age (Myr)
Δt (Myr)
Δt=0
*
**

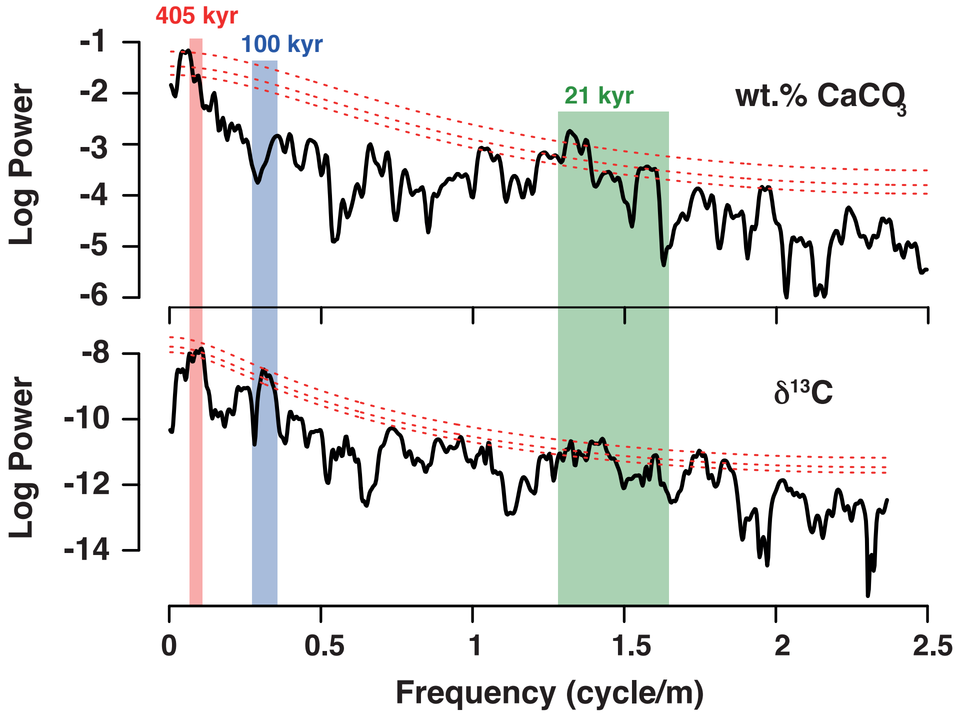
405 kyr
100 kyr
21 kyr
wt.% CaCO3
Log Power
-1
-2
-3
-4
-5
-6
δ13C
Log Power
-8
-10
-12
-14
0
0.5
1
1.5
2
2.5
Frequency (cycle/m)

Figure 5

Figure 6

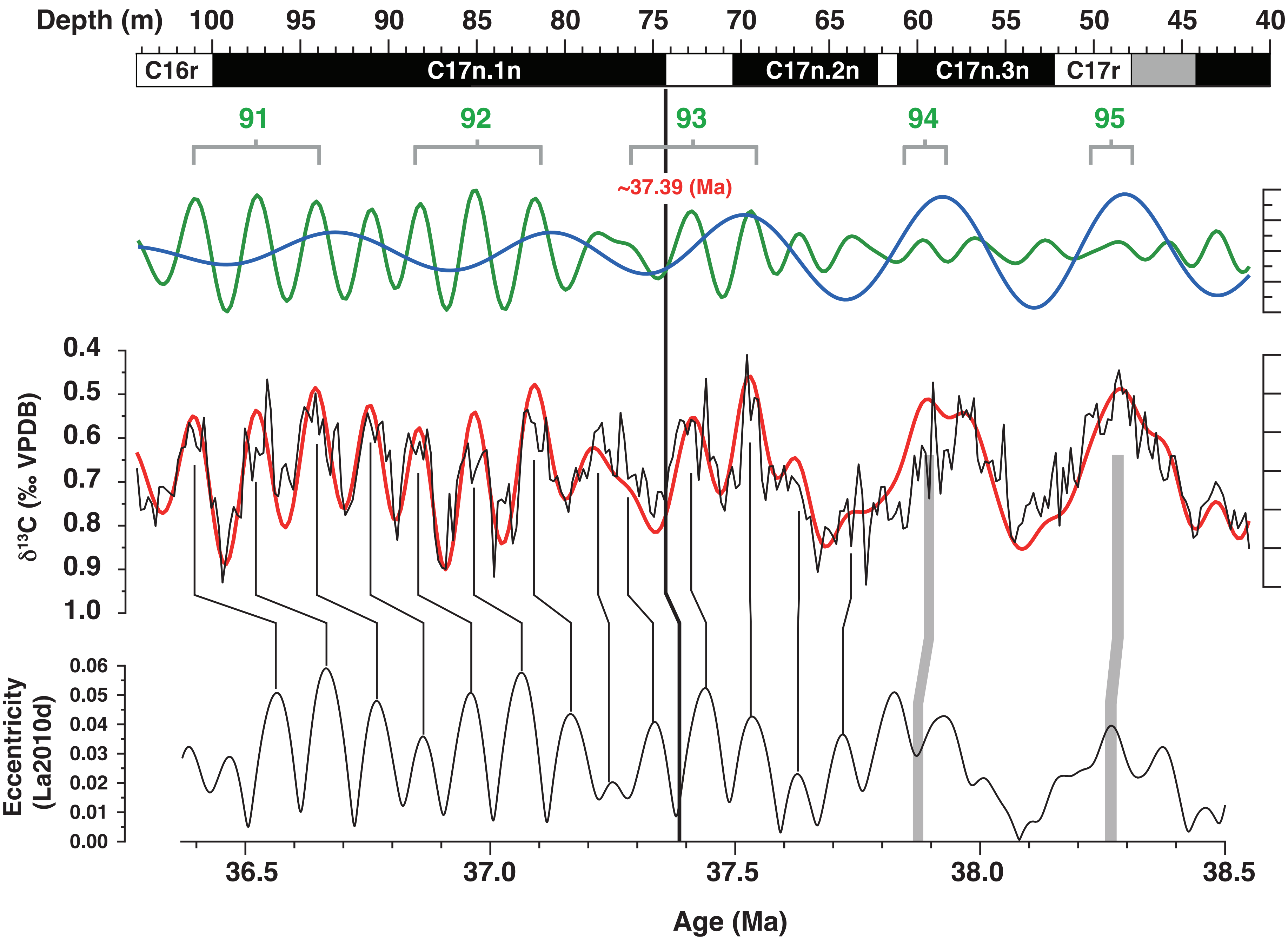

Figure 6

Figure7

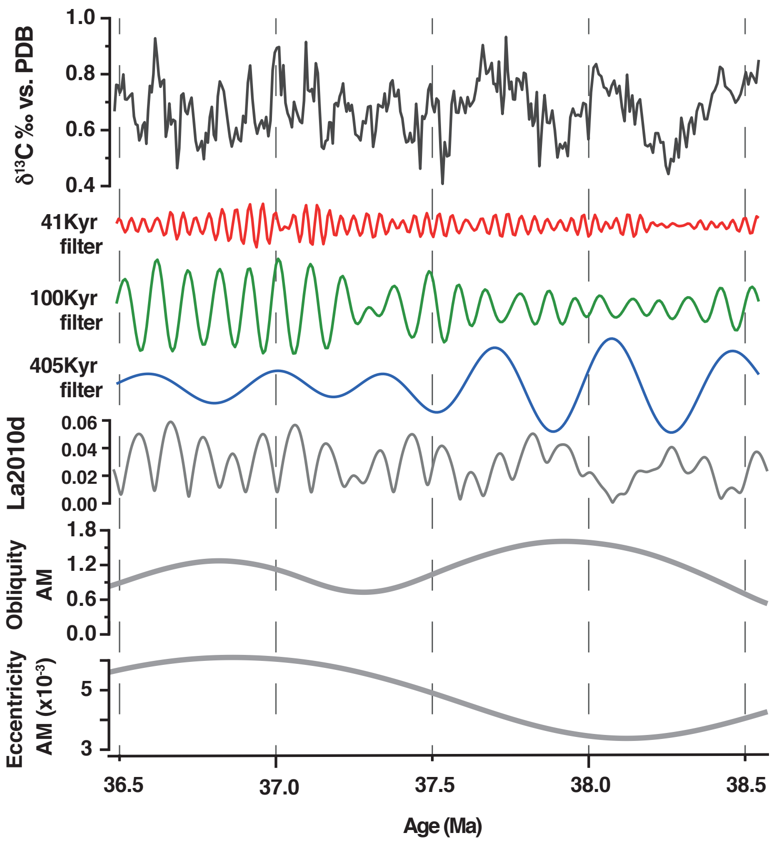

Figure 7

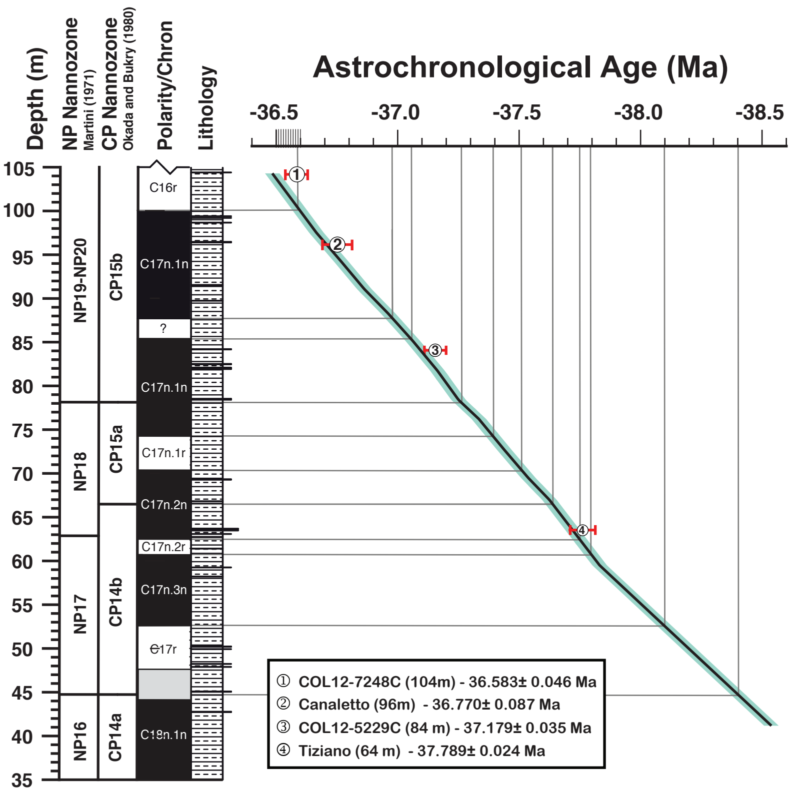

Astrochronological Age (Ma)
-36.5
-37.0
-37.5
-38.0
-38.5
Depth (m)
NP Nannozone
Martini (1971)
CP Nannozone
Okada and Bukry (1980)
Polarity/Chron
Lithology
105
100
95
90
85
80
75
70
65
60
55
50
45
40
35
NP19-NP20
NP18
NP17
NP16
CP15b
CP15a
CP14b
CP14a
C16r
C17n.1n
?
C17n.1n
C17n.1r
C17n.2n
C17n.2r
C17n.3n
C17r
C18n.1n
① COL12-7248C (104m) - 36.583± 0.046 Ma
② Canaletto (96m) - 36.770± 0.087 Ma
③ COL12-5229C (84 m) - 37.179± 0.035 Ma
④ Tiziano (64 m) - 37.789± 0.024 Ma

Figure 8

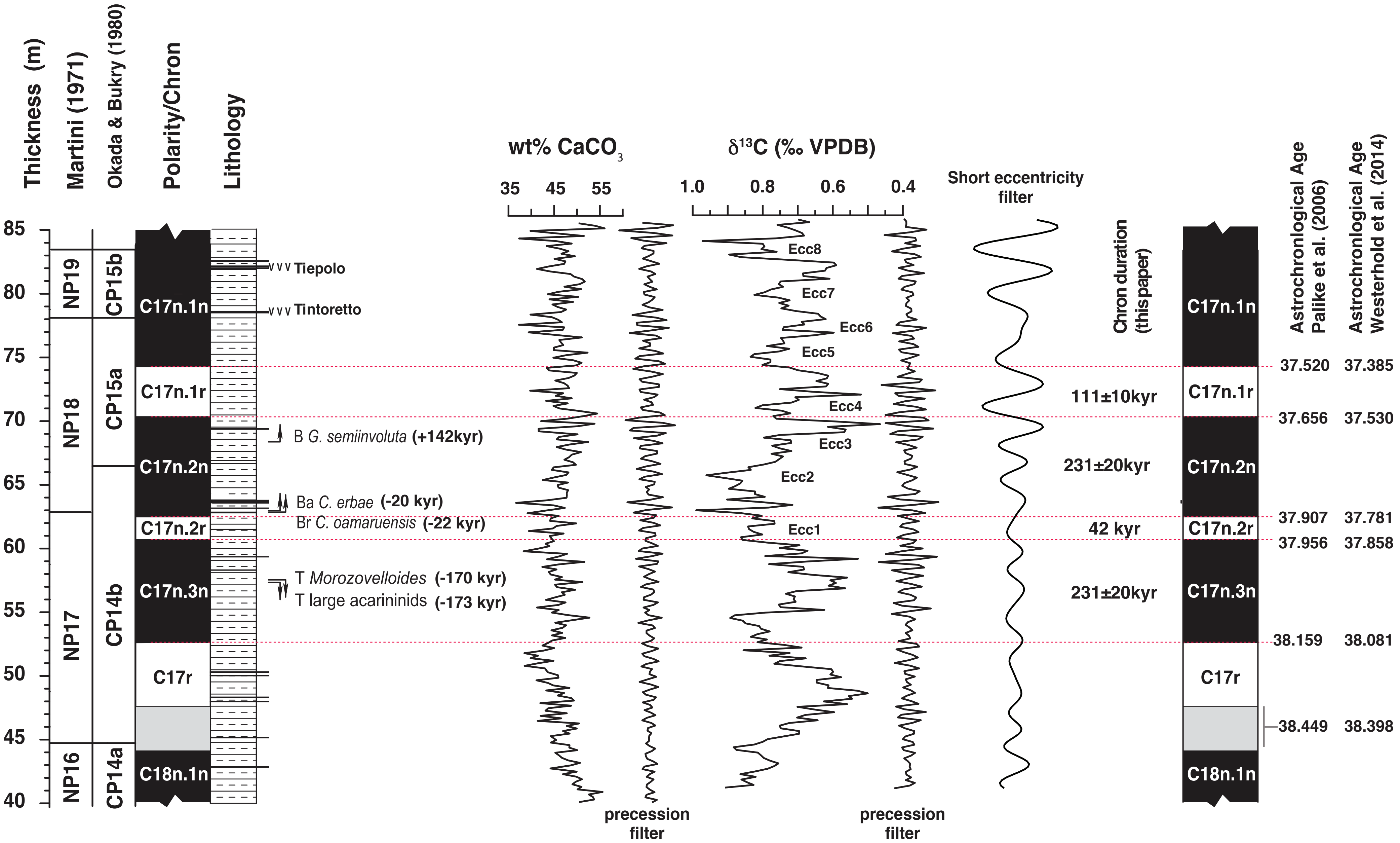
Thickness (m)
Martini (1971)
Okada & Bukry (1980)
Polarity/Chron
Lithology
wt% CaCO3
35 45 55
δ13C (‰ VPDB)
1.0 0.8 0.6 0.4
Short eccentricity filter
Chron duration (this paper)
Astrochronlogical Age Palike et al. (2006)
Astrochronlogical Age Westerhold et al. (2014)
85 80 75 70 65 60 55 50 45 40
NP19 NP18 NP17 NP16
CP15b CP15a CP14b CP14a
C17n.1n C17n.1r C17n.2n C17n.2r C17n.3n C17r C18n.1n
Tiepolo
Tintoretto
B G. semiinvoluta (+142kyr)
Ba C. erbae (-20 kyr)
Br C. oamaruensis (-22 kyr)
T Morozovelloides (-170 kyr)
T large acarininids (-173 kyr)
Ecc8 Ecc7 Ecc6 Ecc5 Ecc4 Ecc3 Ecc2 Ecc1
111±10kyr
231±20kyr
42 kyr
231±20kyr
37.520 37.385
37.656 37.530
37.907 37.781
37.956 37.858
38.159 38.081
38.449 38.398
precession filter
precession filter

Figure 9

Table 1. Arguments in favour of the accuracy of the astronomical age model

Sample	Depth (m)	U-Pb Age (Ma)	U-Pb Age (Ma)*
COL12-7248C	104	36.630± 0.013/0.017/0.046	36.593± 0.046/0.047/0.062
Canaletto	96	36.794± 0.024/0.028/0.048	36.751± 0.064/0.065/0.076
COL12-5229C	84	37.179± 0.015/0.020/0.044	37.154± 0.052/0.053/0.067
Tiziano	64	37.808± 0.018/0.022/0.046	37.762± 0.064/0.065/0.077